Operation of the Zero Ion Backflow electron multiplier in pure argon

PUBLISHED BY IOP PUBLISHING FOR SISSA MEDIALAB

RECEIVED: *August 3, 2014*
ACCEPTED: *November 10, 2014*
PUBLISHED: *December 3, 2014*

Operation of the Zero Ion Backflow electron multiplier in pure argon

F.D. Amaro,[a,1] **C.A.O. Henriques,**[a] **M.R. Jorge,**[a] **A.L.M. Silva**[b] **and E.D.C. Freitas**[a]

[a] *GIAN — Physics Department, University of Coimbra, Coimbra, Portugal*
[b] *I3N — Physics Department, University of Aveiro, Aveiro, Portugal*

E-mail: famaro@gian.fis.uc.pt

ABSTRACT: The operation of the Zero Ion Backflow electron multiplier in pure argon is presented as an alternative to the readout of ionization signals from Time Projection Chambers. The Zero Ion Backflow electron multiplier operates in a noble gas atmosphere and totally suppresses all the secondary ions produced in the electron avalanches. It is composed of a proportional scintillation gap coupled to a gaseous photon-multiplier. The ion backflow suppression of the Zero Ion Backflow electron multiplier was demonstrated to be independent of the total charge gain of the detector. This paper presents the operation of the Zero Ion Backflow electron multiplier in pure argon with a GPM composed by a THCOBRA coupled to a CsI photocathode. For a scintillation gap of 7.5 mm an optical gain close to unity and energy resolution of 35% were achieved, without deterioration of the primary ionization statistical information.

KEYWORDS: Charge transport, multiplication and electroluminescence in rare gases and liquids; Electron multipliers (gas); Particle tracking detectors (Gaseous detectors); Time projection chambers

[1] Corresponding author.

doi:10.1088/1748-0221/9/12/P12002

Contents

1 Introduction 1

2 The Zero Ion Backflow electron multiplier 2

3 Experimental setup 4

4 Results 4

4.1 Optical Gain 5

5 Conclusions 8

2014 JINST 9 P12002

1 Introduction

The standard technique currently employed in Time Projection Chambers (TPC) requiring some level of ion backflow (IBF) suppression is the use of a gating electrode that, once electronically triggered, reverses its polarity and blocks the incoming ions of reaching the sensitive areas of the detector. Otherwise the slowly moving ions would accumulate in the sensitive volume of the detector, were they have the potential to distort the electric field in this region, affecting the tracking properties [1]. This is particularly problematic in high rate TPCs and it is one of the motives for the replacement of wire detectors by micro-patterned gaseous electron multipliers in the ongoing development of the readout elements for the TPC in the future International Linear Collider (ILC) [2, 3].

The development of micro-patterned gaseous electron multipliers such as the Gas Electron Multiplier (GEM) [4], Micromegas [5] and the Micro Hole and Strip Plate (MHSP) [6, 7] lead to a natural reduction of the IBF levels [8]. This is due to their surface with small holes and to the possibility of combining several of these elements in a cascade. So far, to the best of our knowledge, the highest values of IBF suppression achieved in standard gas mixtures were obtained with an MHSP operating in the so-called reversed mode (R-MHSP) [9], making use of the thin strip electrodes present on this micro-structure to trap the ions that flow from the lower stages of a cascade of electron multiplier in which the MHSP is the first element. The operation of the MHSP in the reversed mode allowed to achieve IBF values of 0.03% at a total gain of 10^5 [10]. Despite the strong reduction on the IBF relatively to the wire type electron multipliers (were all the secondary ions are eventually collected at the cathode of the detector and the IBF is 1 [8]) these values fell short of reaching the desired values of IBF $= 1/\mathrm{G}$, being G the total gain of the detector [11]. This figure serves as a rule of thumb, and represents an IBF level similar to the one corresponding to the primary ionization: one ion flowing back to the sensitive region of the detector for each primary electron.

An alternative to IBF reduction that allows for a full IBF suppression is the Zero Ion Backflow electron multiplier [12]. The concept of the Zero Ion Backflow electron multiplier has been already

described in [12] where its operation in pure xenon was reported. It consists of a proportional scintillation region, delimited by two highly transparent metallic meshes, followed by a Gaseous Photomultiplier (GPM). This GPM can be composed of any type of micro-patterned gaseous electron multiplier, coupled to a CsI photocathode. The primary electrons are transferred to the proportional scintillation gap where they are accelerated by an electric field whose value is between the excitation and ionization thresholds of the atoms of the gas. Under this electric field the primary electrons will drift through the scintillation region without any ionization on the gas and therefore without the production of any secondary ions. On the other hand they will emit a copious amount of vacuum ultraviolet (VUV) photons until their collection on the mesh that separates the scintillation gap from the GPM [13, 14]. A fraction of the electroluminescence emitted during the path of the primary electrons thought the scintillation gap is collected by the GPM. Each of the VUV photons that impinge the GPM photocathode has a probability of extracting a photo-electron from the CsI photocathode. The output signal of the GPM is proportional to the number of VUV photons that reach the photocathode and therefore to the energy deposited in the conversion region by the ionizing radiation. A large signal (gains up to 10^4 were achieved with the Zero IBF electron multiplier in pure xenon) can therefore be obtained while at the same time totally suppressing the IBF to the sensitive regions of the detector.

Argon is a common filling gas for many TPC and, being a noble gas, it is suitable for the operation with the Zero IBF electron multiplier. Besides the economic advantage relatively to xenon, argon also presents lower backscattering, reducing the probability that a photo-electron returns to the photocathode once emitted. The quantum efficiency of CsI is also higher for the scintillation wavelength of argon than for xenon. The main drawback in the use of argon in the Zero IBF electron multiplier is the electroluminescence yield in argon being slightly lower than that achieved in xenon [13, 14].

In this paper we investigate the behaviour of the Zero IBF electron multiplier operating in pure argon by recording the pulse height distributions of the output signals as a function the electric fields in the proportional scintillation region, while irradiating the conversion region with 5.9 keV x-rays.

2 The Zero Ion Backflow electron multiplier

A schematic representation of the Zero IBF electron multiplier used in this work is depicted in figure 1. It is composed by an absorption/drift region, limited by the cathode and mesh G1, followed by the proportional scintillation region. This region, 7.5 mm thick, is limited by meshes G1 and G2 and is followed by a 2.5 mm thick extraction region, established between mesh G2 and the GPM. The GPM used in this work was composed by a THCOBRA [15] coupled to a 2500 Å CsI photocathode. An induction electrode is placed 2.5 mm away from the THCOBRA.

The GPM used in the Zero Ion Backflow electron multiplier operating in xenon [12] was a double GEM coupled to a CsI photocathode. However, in this work the double GEM was replaced by a THCOBRA. The THCOBRA is a gaseous electron multiplier made with the same technology of the THGEM [16] being made of a copper clad G10 plate, with holes mechanically drilled. An extra set of electrodes is etched in one of the surfaces of the THCOBRA relatively to a standard THGEM. The THCOBRA is therefore equipped with 3 sets of independent electrodes: the *top*

2014 JINST 9 P12002

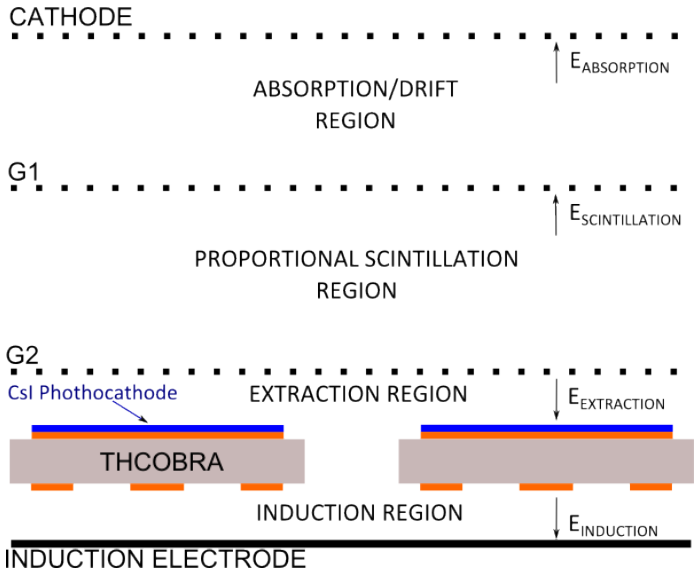

Figure 1. Schematic representation of the Zero IBF detector used in this work.

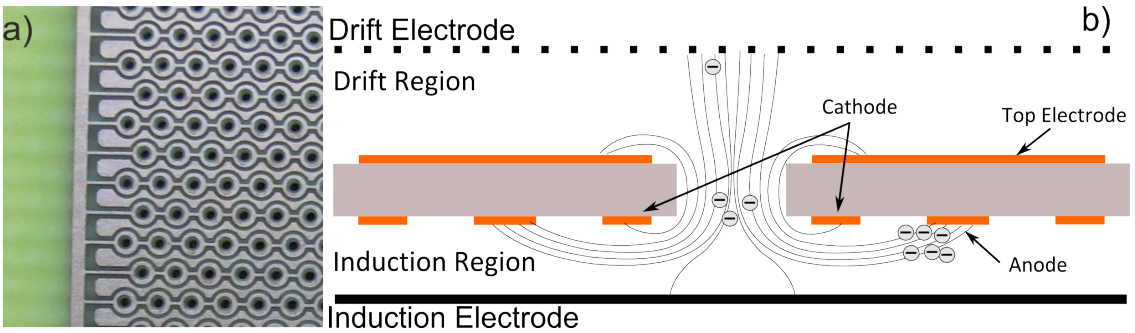

Figure 2. a) Detailed photography of the anode side and cathode side on the THCOBRA. A cathode electrode surrounds each hole. An anode runs between each pair of cathodes. b) Schematic of the THCOBRA operation: a primary electron or photo-electron is focused into one of the holes on the THCOBRA were it is multiplied. The resulting charge is then extracted from the holes and further multiplied in the region around the anodes. The final charge is collected at the anodes.

electrode, which covers one of its surfaces and, on the other surface (figure 2a), the *cathodes* (surrounding the holes in the G10 board) and the *anodes* that run between each pair of cathodes.

These 3 sets of electrodes establish 2 independent multiplication regions in the THCOBRA: one in the region inside the holes, controlled by the voltage difference between the *top* and the *cathode* electrodes (V_{C-T}) and the other between the anode and cathodes, controlled by the voltage difference between *anodes* and *cathodes* (V_{A-C}).

An electron entering the holes in the THCOBRA experiences an intense electric field inside the hole and suffers a first avalanche process in this region, controlled by V_{C-T}. The charge produced is then extracted from this region and further multiplied due to the electric field established in the region between the *anodes* and the *cathodes*. The final charge is collected at the *anodes* of the THCOBRA. For stability purposes a small rim is etched in the copper around the holes of the

2014 JINST 9 P12002

THCOBRA. Gains above 10^4 were achieved in pure argon using a THCOBRA made from a 0.4 mm thick G10 board, with 0.3 mm holes and an active area of $15 \times 15\,mm^2$ [15]. The THCOBRA used in this work has also 0.4 mm thickness and 0.3 mm holes but has an active area of $26 \times 26\,mm^2$.

The electric field, $E_{EXTRACTION}$, established between the CsI photocathode deposited on the *top* electrode of the THCOBRA and the metallic mesh separating the GPM from the scintillation gap plays an important role both in the photo-electron extraction from the photocathode and in the blocking of the secondary ions from the GPM. In [12] it was demonstrated that a value of $E_{EXTRACTION}$ between 0.1 and $0.2\,kV \times cm^{-1} \times bar^{-1}$ ensures simultaneously full IBF suppression and maximum photo-electron extraction efficiency from the photocathode.

3 Experimental setup

The Zero IBF detector has been investigated within a stainless steel vessel, with pure argon (Linde, 99.9993%) at a pressure of 1.1 bar. Prior to the gas filling the stainless steel chamber was evacuated down to 10^{-6} mbar. After filling the detector with gas, the argon was purified by circulation through non-evaporable getters, SAES St707, placed in an adjacent volume to the detector and kept at 200°C. The electrical connections are made of high vacuum compatible MACOR feedthroughs and the electrodes of the detector were independently polarized using CAEN N471A power supplies with current limitation (100 nA).

All the meshes used in the Zero IBF electron multiplier (cathode, G1 and G2 in figure 1) are stainless steel meshes made of 80 μm diameter wires with 900 μm spacing.

The 5.9 keV x-rays emitted by a ^{55}Fe source were used to produce the primary electron clouds in the absorption/drift region. A 0.015 mm thick Cr film was used to filter the 6.49 keV k_β line also emitted by the ^{55}Fe source. The final avalanche-charge produced on each event was recorded from the anodes of the THCOBRA using a Canberra 2006 charge-sensitive preamplifier (sensitivity set to 47 mV/MeV) followed by a Tennelec TC 243 linear amplifier (4 μs shaping time) and a Nucleus PCA 2 multichannel analyzer. The electronic chain sensitivity was calibrated by injection of a known charge into the preamplifier input.

4 Results

The behaviour of the Zero IBF electron multiplier operating in pure argon was investigated by irradiating the absorption/drift region with x-rays emitted from ^{55}Fe radioactive source. The charge gains achieved with the THCOBRA in argon were determined by measuring the direct signal from the x-rays converted in the gap between the THCOBRA and G2. For this purpose the electric fields in the scintillation and extraction regions were reversed relatively to the directions pointed in figure 1. Under this electric field configuration all the primary electron clouds resulting from the interactions taking place in the scintillation region are collected at mesh G1 and not multiplied in the GPM. Only the x-rays that are not absorbed in the scintillation region and that convert in the extraction region (figure 1) are multiplied in the THCOBRA.

In figure 3 we present the charge gain achieved with the THCOBRA as a function of the voltage difference between the anode and cathodes (V_{A-C}) for different voltage differences between the top and the cathode electrodes (V_{C-T}).

2014 JINST 9 P12002

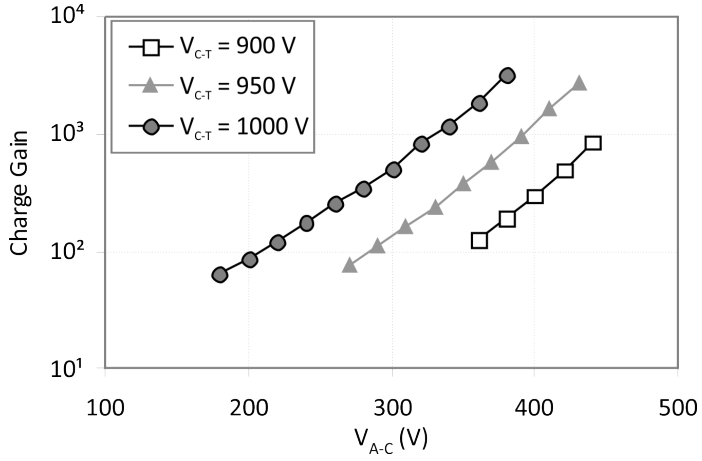

Figure 3. Charge gain of the THCOBRA as a function of the voltages applied in the THCOBRA, measured from the 5.9 keV x-rays interacting in the extraction region of the Zero IBF electron multiplier. The electric field in the extraction region was reversed, relative to the normal operation of the Zero IBF electron multiplier.

Maximum charge gains above 10^3 were achieved with the THCOBRA in the present work. This value is one order of magnitude lower than the one achieved in [12] using a THCOBRA without a CsI photocathode. The difference in the maximum gain achievable is due to the limitation on the maximum voltages possible to be applied to this THCOBRA as, for similar voltages, the gains of figure 3 are consistent with the ones obtained in [12]. A limitation on the charge gain achieved in gaseous electron multipliers when operating in pure noble gases has been reported in [17] and is the main reason why, for the operation in pure argon, the double GEM electron multiplier used in [12] was replaced by a THCOBRA. A double GEM electron multiplier was initially tested in pure argon and failed to provide the necessary charge gains to operate. The THCOBRA, despite the limitations on the maximum voltage applicable, provided maximum gains above 10^3 and allowed the operation of the Zero IBF in pure argon.

Figure 4 presents a typical pulse height distribution of the direct signal, obtained with the Zero IBF electron multiplier when irradiating the extraction region with 5.9 keV x-rays from a ^{55}Fe x-ray source. The electric fields in the conversion/drift region, in the scintillation region and in the extraction region were set to $0.5\,\mathrm{kV}\times\mathrm{cm}^{-1}\times\mathrm{bar}^{-1}$, $-0.35\,\mathrm{kV}\times\mathrm{cm}^{-1}\times\mathrm{bar}^{-1}$ and $-0.30\,\mathrm{kV}\times\mathrm{cm}^{-1}\times\mathrm{bar}^{-1}$, respectively (signals are relative to the electric field configuration of figure 1). With this configuration only the x-rays converted in the 2.5 mm extraction region are multiplied in the THCOBRA. The voltage difference between top and cathode (V_{C-T}) and between cathode and anode (V_{A-C}) on the THCOBRA were respectively 900 and 400 V. The voltage on the induction electrode was set to 900 V. An energy resolution of 45% was measured at 5.9 keV.

4.1 Optical Gain

The optical gain of the Zero IBF electron multiplier is defined as the number of photo-electrons extracted from the CsI photocathode and further multiplied in the GPM per each primary electron converted in the drift region. This figure can be directly obtained from the ratio between the amplitude of the scintillation pulses, as read by the GPM, for the 5.9 keV X-ray interactions in the

2014 JINST 9 P12002

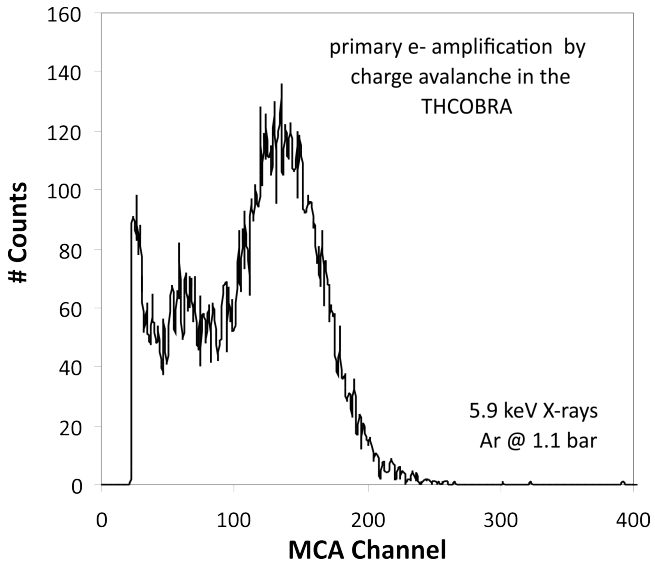

Figure 4. Pulse height distribution obtained with the THCOBRA. Charge gain of 400 and energy resolution of 45% were measured for the 5.9 keV x-rays from the ^{55}Fe source.

conversion region and the charge signal resulting from interactions in the extraction region and amplified on the THCOBRA, when the electric fields in the scintillation and extraction regions are reversed, as described above.

The scintillation peak is obtained in the standard operation mode of the Zero IBF electron multiplier, with the electric fields in the absorption/drift and scintillation regions pointing in the directions represented in figure 1. The electric field in the extraction region was set to $0.1\,\mathrm{kV} \times \mathrm{cm}^{-1} \times \mathrm{bar}^{-1}$, while the electric field in the scintillation region was $2.9\,\mathrm{kV} \times \mathrm{cm}^{-1} \times \mathrm{bar}^{-1}$. Figure 5 presents a typical pulse height distribution obtained in such conditions (blue curve). The voltages applied on the THCOBRA were the same as the ones used for the direct peak presented in figure 4.

Due to the small depth of the absorption/drift region used in our setup (4.5 mm) not all the x-rays crossing this region are absorbed there. A large number is converted in the scintillation region. Since the secondary scintillation is emitted uniformly along the path of the primary electrons, interactions taking place deeper in the scintillation region will translate into a lower amplitude signal at the output of the detector. The scintillation peak recorded under such conditions is affected by a tail towards low energy (blue curve in figure 5). In order to eliminate the contribution of the x-rays absorbed in the scintillation region the electric field in the absorption/drift region have been reversed, recording only the pulses converted in the scintillation region (red curve, figure 5). Then this pulse height distribution was subtracted to the scintillation peak in order to obtain the signal corresponding only to the interactions taking place in the absorption/drift region (black curve, figure 5). The fitting of a Gaussian curve to this spectra yields and energy resolution of 34% (FWHM). This figure is compared to the 45% measured for the direct peak and translates the improvement in the statistics when the scintillation region is polarized.

Figure 6 presents the optical gain (grey squares; left axis) and the energy resolution (grey circles; right axis) achieved with the Zero IBF electron multiplier operating in argon. For comparison the values for the optical gain measured in pure xenon [12] are also presented (white triangles;

2014 JINST 9 P12002

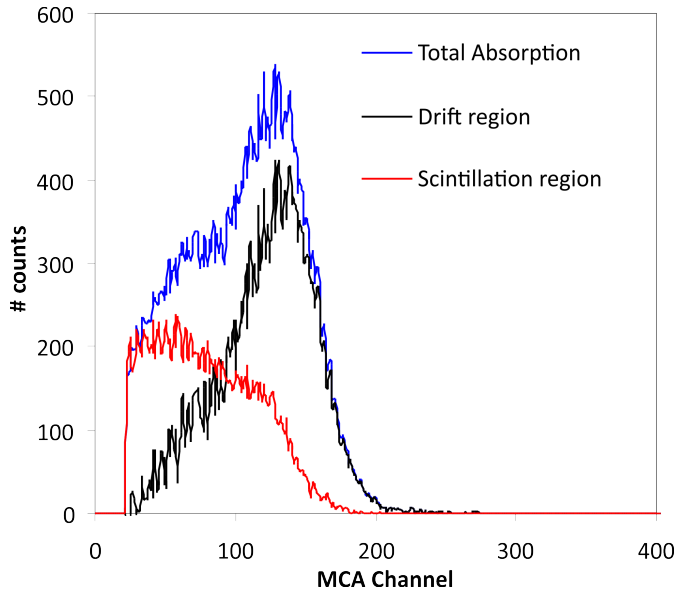

Figure 5. Pulse height distribution obtained with Zero IBF electron multiplier when irradiated with 5.9 keV x-rays. Blue: conversions taking place in the drift and in the scintillation region. Red: interactions that take place only in the scintillation region; the output signal depends on the depth were the interaction took place. Black: interactions taking place only in the drift/absorption region.

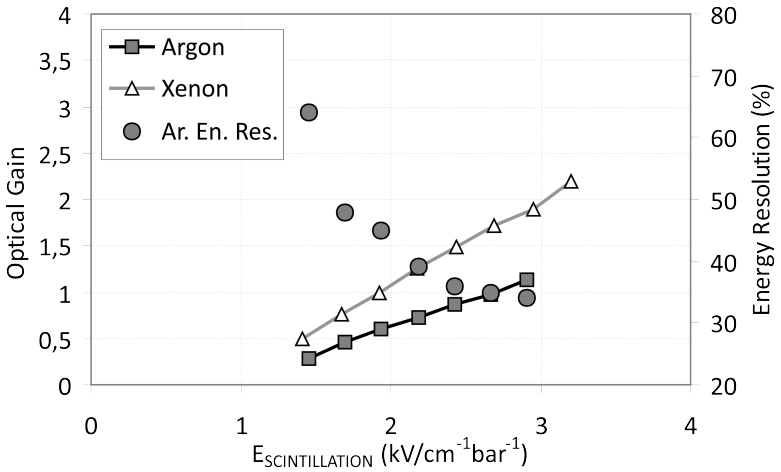

Figure 6. Optical gain and energy resolution achieved with the Zero IBF electron multiplier operating in pure argon. The optical gain measured in pure xenon [12] is also included for comparison.

left axis). In both cases the optical gain follows the same trend as the secondary scintillation in a uniform field [13, 14]. Besides the secondary scintillation yield of the gas (higher in xenon than in argon) the optical gain is also dependent on the CsI quantum efficiency and on the photo-electron extraction efficiency as well as other geometrical factors such as the mesh transparency (83%), the average solid angle covered by the photocathode (0.37) and the active area of the THCO-BRA were the photocathode was deposited (80%). All these factors result in a slightly lower optical gain when compared with the value obtained in xenon, for the same $E_{SCINTILLATION}$. One

2014 JINST 9 P12002

would expect the lower scintillation yield in argon [13, 14] to be somewhat compensated by the higher photo-electron extraction efficiency (0.45 for argon vs. 0.25 for xenon, for an electric field of $1.0\,\mathrm{V}\times\mathrm{cm}^{-1}\times\mathrm{torr}^{-1}$ [18]) and by the higher CsI quantum efficiency for the 128 nm argon secondary scintillation wavelength [19]. Unfortunately, no precise data were available concerning the CsI quantum efficiency for the argon secondary scintillation wavelength (128 nm) which depends strongly of the photo-electron extraction efficiency [18].

The energy resolution achieved with the Zero IBF electron multiplier reaches values of 34% for an electric field above $2.5\,\mathrm{kV}\times\mathrm{cm}^{-1}\times\mathrm{bar}^{-1}$. These values compare favourably with the ones obtained for the direct peak with the THBCOBRA (45%) and show that the introduction of a first stage of proportional scintillation production, combined with a CsI photocathode for scintillation readout, does not degrade the energy resolution and overall response of the electron multiplier, even for an optical gain of ~ 1 as the one measured for $\mathrm{E}_{\mathrm{SCINTILLATION}} = 2.5\,\mathrm{kV}\times\mathrm{cm}^{-1}\times\mathrm{bar}^{-1}$. In addition, provided the electric insulation of the different electrodes allows, one could increase $\mathrm{E}_{\mathrm{SCINTILLATION}}$ up to values of $4\,\mathrm{kV}\times\mathrm{cm}^{-1}\times\mathrm{bar}^{-1}$, without having charge multiplication in the scintillation region [13], increasing the optical gain and further improving the energy resolution.

5 Conclusions

We presented the operation of the Zero Ion Backflow electron multiplier in pure argon. Optical gains slightly lower than the ones obtained in pure xenon were achieved, reaching a value of 1 for an electric field of $2.5\,\mathrm{kV}\times\mathrm{cm}^{-1}\times\mathrm{bar}^{-1}$ in the scintillation region. Even for such low gains associated with the secondary scintillation stage an energy resolution of 35% FWHM was achieved for 5.9 keV x-rays. This figure compares favourably with the one achieved without the secondary scintillation stage (45%), measured for the same voltages on the THCOBRA. Even for an optical gain of only 1 there is an improvement in the statistical information with the inclusion of a proportional scintillation stage. If necessary the optical gain of the Zero IBF electron multiplier can be improved by increasing the proportional scintillation gap thickness, the gas pressure and/or the effective area of the CsI photocathode. Mixtures or argon with small amounts of xenon are known to combine a high scintillation output with low electron backscattering, and are therefore expected to provide higher optical gain and will be studied in a near future. A small amount, of the order of 1% of CH_4 added to pure argon may also provide higher photoelectron extraction efficiency and more stable operation of the GPM charge gain, with a controlled loss in the scintillation yield of this mixture.

Acknowledgments

This work is funded by FEDER, through the Programa Operacional Factores de Competitividade-COMPETE and by National funds through FCT- Fundação para a Ciência e Tecnologia in the frame of project CERN/FP/123614/2011. Fernando D. Amaro was supported by FCT under Post-Doctoral Grant SFRH/BPD/74775/2010.

2014 JINST 9 P12002

References

[1] A. Bagulya et al., *Dynamic Distortions in the HARP TPC: Observations, measurements, modelling and corrections*, 2009 *JINST* **4** P11014 [arXiv:0903.4762].

[2] ILD CONCEPT GROUP collaboration, T. Abe et al., *The International Large Detector: Letter of Intent*, arXiv:1006.3396.

[3] LCTPC collaborationtpc, *R&D for a Linear Collider Detector*, Status Report, April 2008.

[4] F. Sauli, *GEM: A new concept for electron amplification in gas detectors*, *Nucl. Instrum. Meth.* **A 386** (1997) 531.

[5] G. Charpak, J. Derre, Y. Giomataris and P. Rebourgeard, *MicrOMEGAs, a multipurpose gaseous detector*, *Nucl. Instrum. Meth.* **A 478** (2002) 26.

[6] J.F.C.A. Veloso, J.M.F. Dos Santos and C.A.N. Conde, *A proposed new microstructure for gas radiation detectors: The microhole and strip plate*, *Rev. Sci. Instrum.* **71** (2000) 2371.

[7] J.M. Maia, J.F.C.A. Veloso, J.M.F. Dos Santos, A. Breskin, R. Chechik and D. Mörmann, *Advances in the Micro-Hole & Strip Plate gaseous detector*, *Nucl. Instrum. Meth.* **A 504** (2003) 364.

[8] A. Breskin et al., *Ion-induced effects in GEM and GEM/MHSP gaseous photomultipliers for the UV and the visible spectral range*, *Nucl. Instrum. Meth.* **A 553** (2005) 46 [physics/0502132].

[9] J.F.C.A. Veloso et al., *MHSP in reversed-biased operation mode for ion blocking in gas-avalanche multipliers*, *Nucl. Instrum. Meth.* **A 548** (2005) 375 [physics/0503237].

[10] A. Lyashenko, A. Breskin, R. Chechik, F.D. Amaro, J.F.C.A. Veloso and J.M.F. Dos Santos, *High-gain DC-mode operated Gaseous Photomultipliers for the visible spectral range*, *Nucl. Instrum. Meth.* **A 610** (2009) 161 [arXiv:0808.1556].

[11] F. Sauli, L. Ropelewski and P. Everaerts, *Ion feedback suppression in time projection chambers*, *Nucl. Instrum. Meth.* **A 560** (2006) 269.

[12] F.D. Amaro, M. Ball, J.F.C.A. Veloso and J.M.F. Dos Santos, *Zero Ion Backflow electron multiplier operating in noble gases*, 2014 *JINST* **9** P02004.

[13] C.M.B. Monteiro, J.A.M. Lopes, J.F.C.A. Veloso and J.M.F. Dos Santos, *Secondary scintillation yield in pure argon*, *Phys. Lett.* **B 668** (2008) 167.

[14] C.M.B. Monteiro et al., *Secondary Scintillation Yield in Pure Xenon*, 2007 *JINST* **2** P05001 [physics/0702142].

[15] F.D. Amaro, C. Santos, J.F.C.A. Veloso, A. Breskin, R. Chechik and J.M.F. Dos Santos, *The Thick-COBRA: A New Gaseous Electron Multiplier for Radiation Detectors*, 2010 *JINST* **5** P10002 [arXiv:1008.0830].

[16] A. Breskin et al., *A concise review on THGEM detectors*, *Nucl. Instrum. Meth.* **A 598** (2009) 107 [arXiv:0807.2026].

[17] J. Miyamoto, A. Breskin and V. Peskov, *Gain limits of a Thick GEM in high-purity Ne, Ar and Xe*, 2010 *JINST* **5** P05008 [arXiv:1001.4741].

[18] L.C.C. Coelho et al., *Measurement of the photoelectron-collection efficiency in noble gases and methane*, *Nucl. Instrum. Meth.* **A 581** (2007) 190.

[19] A. Breskin, *CsI UV photocathodes: History and mystery*, *Nucl. Instrum. Meth.* **A 371** (1996) 116.

2014 JINST 9 P12002